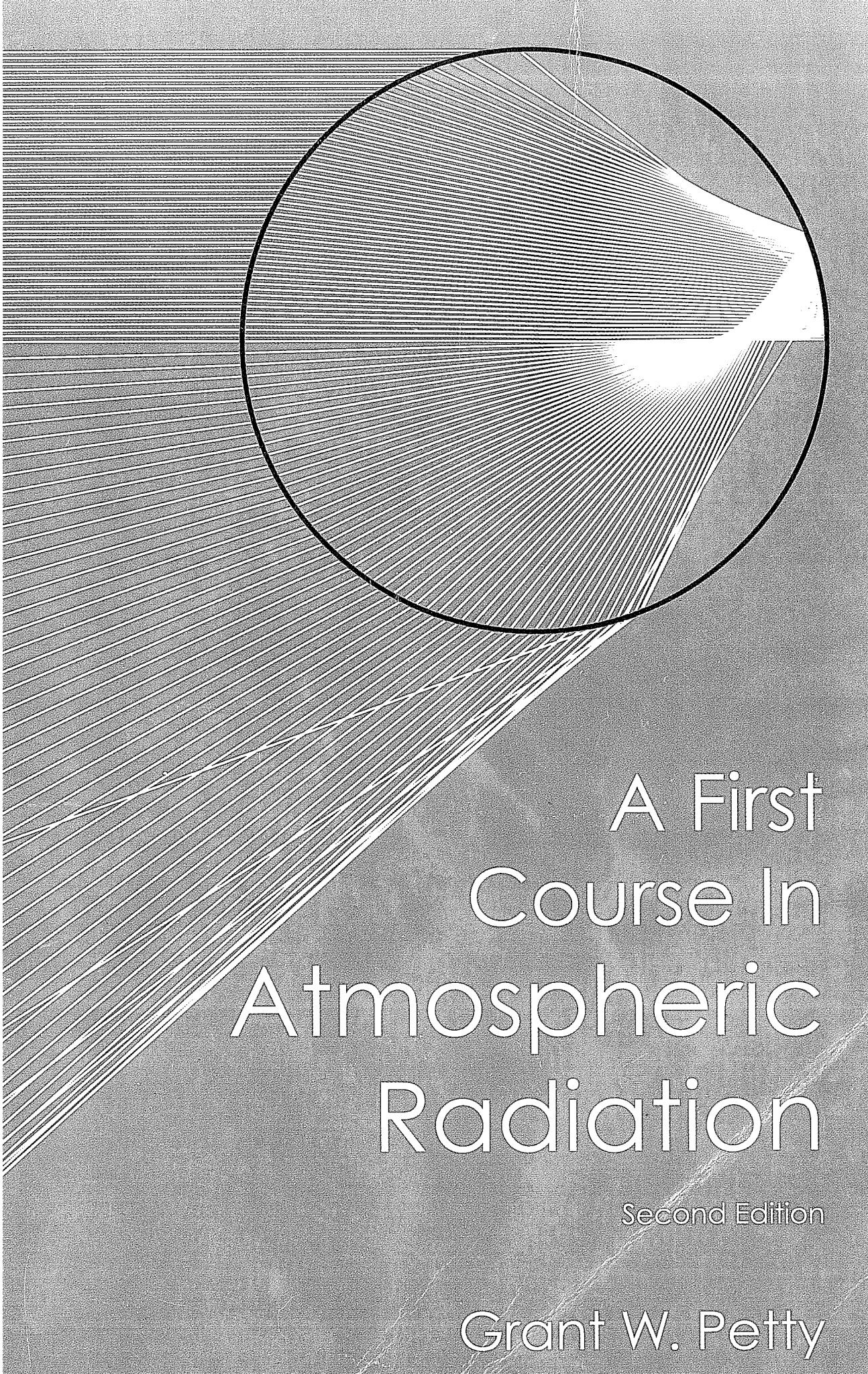

A First Course In Atmospheric Radiation

Second Edition

Grant W. Petty

CHAPTER 8

Atmospheric Emission

In the previous chapter, we began our examination of how monochromatic radiation interacts with the atmosphere, focusing initially on the *extinction* (or, conversely, *transmission*) of radiation by atmospheric gases and clouds. If the depletion by the atmosphere of radiation from an external source, such as the sun, were the only process we had to worry about, life would be simple indeed. But we already know from our previous discussion of simple radiative balance models that the atmosphere both absorbs and emits radiation. And we already hinted that Kirchhoff's Law implies a correspondence between absorption and emission that is just as valid for the atmosphere as it is for a solid surface.

We are now ready to expand our understanding of radiative transfer to include both extinction and thermal emission. Eventually, we will also have to come to grips with the problem of scattering as another potential source of radiation along a particular line of sight. But that is a subject for a later chapter. In this chapter, we will restrict our attention to problems in which scattering can be safely ignored. This is not an unreasonable approach for the majority of real-world problems involving the thermal IR, far IR, or microwave bands.

8.1 Schwarzschild's Equation

Consider the passage of radiation of wavelength λ through a layer of air with infinitesimal thickness ds, measured along the direction of propagation. If the radiant intensity is initially I, then the reduction in I due to absorption is

$$dI_{\text{abs}} = -\beta_{\text{a}} I \, ds \, , \tag{8.1}$$

where we are using (7.4) applied to the case that the single scatter albedo $\tilde{\omega} = 0$ and therefore $\beta_{\text{e}} = \beta_{\text{a}}$.

The quantity $\beta_{\text{a}} ds$ can be thought of as the absorptivity a of the thin slice of the medium, since it describes the fraction of the incident radiation that is lost to absorption. But Kirchhoff's Law tells us that the absorptivity of any quantity of matter in local thermodynamic equilibrium (LTE) is equal to the emissivity of the same matter. Therefore, we can expect the thin layer of air to *emit* radiation in the amount

$$dI_{\text{emit}} = \beta_{\text{a}} B \, ds \, , \tag{8.2}$$

where we are using the symbol B here as a convenient short-hand[1] for the Planck function $B_\lambda(T)$. The *net* change in radiant intensity is therefore

$$dI = dI_{\text{abs}} + dI_{\text{emit}} = \beta_{\text{a}} (B - I) \, ds \, , \tag{8.3}$$

or

$$\boxed{\frac{dI}{ds} = \beta_{\text{a}} (B - I) \, .} \tag{8.4}$$

This equation is known as *Schwarzschild's Equation* and is the most fundamental description of radiative transfer in a nonscattering medium. Schwarzschild's Equation tells us that the radiance along a particular line of sight either increases or decreases with distance traveled, depending on whether $I(s)$ is less than or greater than $B[T(s)]$, where $T(s)$ is the temperature at point s.

Let us now consider the intensity of radiation arriving at a particular sensor looking backward along the direction of propagation.

[1] Note that we have also dropped the subscript λ from I and other quantities, as all relationships discussed in this chapter should be understood as applying to radiative transfer at a single wavelength.

Much as we did previously for a plane parallel atmosphere, we can introduce

$$\tau(s) = \int_s^S \beta_a(s')\, ds' \tag{8.5}$$

as the *optical path* between an arbitrary point s and the sensor positioned at S. By this definition, $\tau(S) = 0$. Differentiating yields

$$d\tau = -\beta_a\, ds\,, \tag{8.6}$$

which, when substituted into Schwarzschild's Equation, gives

$$\frac{dI}{d\tau} = I - B\,. \tag{8.7}$$

We can integrate this equation by multiplying both sides by the integrating factor $e^{-\tau}$ and noting that

$$\frac{d}{d\tau}[Ie^{-\tau}] = e^{-\tau}\frac{dI}{d\tau} - Ie^{-\tau}\,, \tag{8.8}$$

so that

$$e^{-\tau}\frac{dI}{d\tau} - Ie^{-\tau} = -Be^{-\tau} \tag{8.9}$$

becomes

$$\frac{d}{d\tau}[Ie^{-\tau}] = -Be^{-\tau}\,. \tag{8.10}$$

We then integrate with respect to τ between the sensor at $\tau = 0$ and some arbitrary point τ':

$$\int_0^{\tau'} \frac{d}{d\tau}[Ie^{-\tau}]\, d\tau = -\int_0^{\tau'} Be^{-\tau}\, d\tau\,, \tag{8.11}$$

which simplifies to

$$[I(\tau')e^{-\tau'}] - I(0) = -\int_0^{\tau'} Be^{-\tau}\, d\tau \tag{8.12}$$

or

$$\boxed{I(0) = I(\tau')e^{-\tau'} + \int_0^{\tau'} Be^{-\tau}\, d\tau\,.} \tag{8.13}$$

Let's stop a moment and carefully study this equation, because it is remarkably far-reaching in its implications for radiative transfer. On the left hand side is $I(0)$ which is the radiant intensity observed by the sensor stationed at $\tau = 0$. On the right hand side are two terms:

1. The intensity I at position $\tau = \tau'$, multiplied by the transmittance $t(\tau') = e^{-\tau'}$ between the sensor and τ'. This term therefore represents the attenuated contribution of any radiation source on the far side of the path. For example, for a downward-viewing satellite sensor, $I(\tau')$ could represent emission from the earth's surface, in which case $e^{-\tau'}$ is the total atmospheric transmittance along the line-of-sight.

2. The integrated thermal emission contributions $Bd\tau$ from each point τ along the line of sight between the sensor and τ'. Again, these contributions are attenuated by the respective path transmittances between the sensor and τ', hence the appearance of $t(\tau) = e^{-\tau}$ inside the integral.

Although we went through some minor mathematical gymnastics to get to this point, our analysis of the resulting equation is in fact consistent with a common-sense understanding of how radiation "ought" to work. Among other things, (8.13) tells us that $I(0)$ is not influenced by emission from points for which the intervening atmosphere is opaque ($t \approx 0$). It also tells us that, in order to have emission from a particular point along the path, β_a must be nonzero at that point, since otherwise $d\tau$, and therefore $Bd\tau$, is zero.

Key Point: *Almost all common radiative transfer problems involving emission and absorption in the atmosphere (without scattering) can be understood in terms of (8.13)!*[2]

Let us try to gain more insight into (8.13) by rewriting it in a couple of different forms. Let's start by using the fact that $t = e^{-\tau}$, so that

$$dt = -e^{-\tau}\, d\tau\,. \tag{8.14}$$

[2]The only exceptions are those in which local thermodynamic equilibrium (LTE) doesn't apply, as discussed in Section 6.2.3.

With these substitutions, we now have

$$\boxed{I(0) = I(\tau')t(\tau') + \int_{t(\tau')}^{1} B dt \,.} \tag{8.15}$$

With this form, we can see that equal increments of changing transmittance along the line of sight carry equal weight in determining the total radiance seen at $\tau = 0$.

Finally, let's consider the relative contribution of emission as a function of geometric distance s along the path. Noting that

$$dt = \frac{dt}{ds} ds \,, \tag{8.16}$$

we have

$$I(S) = I(s_0)t(s_0) + \int_{s_0}^{S} B(s) \frac{dt(s)}{ds} ds \,, \tag{8.17}$$

where s_0 is the geometric point that coincides with our chosen optical limit of integration τ'. Comparing this form with (7.55), it suddenly dawns on us that the integral on the right hand side can be written

$$\int_{s_0}^{S} B(s) \frac{dt(s)}{ds} ds = \int_{s_0}^{S} B(s) W(s) ds \,, \tag{8.18}$$

where the *weighting function* $W(s)$ for thermal emission is *exactly the same as the weighting function for absorption of radiation traveling in the opposite direction!*

A Digression on the Emission Weighting Function†

Let us take a minute to show how general the above result really is. Although our focus in this chapter is on the atmosphere, the validity of $W(s) = dt(s)/ds$ as a measure of where emitted radiation is coming from is not restricted to the atmosphere. Consider, for example, the surface of an opaque, perfectly absorbing medium positioned at s', such that the transmittance between an external point and arbitrary s is a step function; i.e.,

$$t(s) = \begin{cases} 1 & s > s' \\ 0 & s < s' \end{cases} \tag{8.19}$$

For this case $dt(s)/ds \equiv W(s) = 0$ for any $s \neq s_0$ and infinite for $s = s'$. In fact, we can write

$$W(s) = \delta(s - s') \,, \tag{8.20}$$

where $\delta(x)$ is the Dirac δ-function. If you have not heard of this function before, then let me quickly summarize its key properties:

$$\delta(x) = \begin{cases} \infty & x = 0 \\ 0 & x \neq 0 \end{cases} \tag{8.21}$$

In other words, $\delta(x)$ is a function that is zero everywhere except at $x = 0$, where it is an infinitely tall, infinitely narrow spike. Despite these unusual properties, the area under the curve is defined to be finite and equal to one. That is,

$$\int_{-\infty}^{x} \delta(x - x')\, dx' = \begin{cases} 0 & x < x' \\ 1 & x > x' \end{cases} \tag{8.22}$$

This is of course consistent with (8.19) and (8.20).

Now if you think about it a bit, you will realize that the product of $\delta(x - x')$ with $f(x')$ is just the same δ-function, but multiplied by the value of $f(x = x')$. Thus, (8.22) implies

$$\int_{x_1}^{x_2} \delta(x - x') f(x')\, dx' = \begin{cases} f(x) & x_1 < x < x_2 \\ 0 & \text{otherwise} \end{cases} \tag{8.23}$$

Let us now look at what this implies for (8.18), given (8.20):

$$I(S) = I(s_0)t(s_0) + \int_{s_0}^{S} B(s)\delta(s - s')ds \,, \tag{8.24}$$

where we will take s_0 to be an arbitrary point below our surface at s', so that $s_0 < s' < S$. Since the medium in question is opaque by assumption, the transmittance $t(s_0) = 0$, and we're left with

$$I(S) = \int_{s_0}^{S} B(s)\delta(s - s')ds \,, \tag{8.25}$$

or, invoking (8.23),

$$I(S) = B(s') \,. \tag{8.26}$$

We have just confirmed, in an admittedly roundabout way, what we already knew: The emitted intensity from a opaque blackbody is just the Planck function B evaluated at the surface of the blackbody. Why did we go to all this trouble? My purpose was simply to demonstrate that (8.17) is quite general (for a nonscattering and nonreflecting medium) and is valid even when the transmittance t is a discontinuous function of distance along a path.

8.2 Radiative Transfer in a Plane Parallel Atmosphere

Let us now adapt (8.17) to a plane-parallel atmosphere. We will start by considering the case that a sensor is located at the surface ($z = 0$), viewing downward emitted radiation from the atmosphere. The appropriate form of the radiative transfer equation is then

$$\boxed{I^{\downarrow}(0) = I^{\downarrow}(\infty)t^* + \int_0^{\infty} B(z)W^{\downarrow}(z)dz\,,} \tag{8.27}$$

where $z = \infty$ represents an arbitrary point beyond the top of the atmosphere, and $t^* \equiv \exp(-\tau^*/\mu)$ is the transmittance from the surface to the top of the atmosphere. Recall that we are using $B(z)$ here as a shorthand for $B_\lambda[T(z)]$, where $T(z)$ is the atmospheric temperature profile. Because the transmittance $t(0,z)$ between the surface and altitude z decreases with increasing z, our weighting function $W^{\downarrow}(z)$ in this case is given by

$$\boxed{W^{\downarrow}(z) = -\frac{dt(0,z)}{dz} = \frac{\beta_a(z)}{\mu}t(0,z)\,.} \tag{8.28}$$

Unless the sensor is pointing at an extraterrestrial source of radiation, such as the sun, $I^{\downarrow}(\infty) = 0$. In this case, the first term on the right vanishes, and the observed downward intensity is strictly a function of the atmospheric temperature and absorption profiles.

Now let's consider a sensor above the top of the atmosphere looking down toward the surface. We then have

$$\boxed{I^{\uparrow}(\infty) = I^{\uparrow}(0)t^* + \int_0^{\infty} B(z)W^{\uparrow}(z)dz\,,} \tag{8.29}$$

where

$$\boxed{W^{\uparrow}(z) = \frac{dt(z,\infty)}{dz} = \frac{\beta_a(z)}{\mu}t(z,\infty)\,.} \tag{8.30}$$

Note the strong similarity between (8.27) and (8.29). Both state that the radiant intensity emerging from the bottom or top of the atmosphere is the sum of two contributions: 1) the transmitted radiation entering the atmosphere from the opposite side, and 2) a weighted sum of the contributions of emission from each level z within the atmosphere.

8.2.1 The Emissivity of the Atmosphere

Consider the case that $T(z) = T_a$, where T_a is the temperature of an isothermal atmosphere. Then $B[T(z)] = B(T_a) = constant$, so that (8.27), together with (8.28), can be written

$$I^{\downarrow}(0) = I^{\downarrow}(\infty)t^* + B(T_a)\int_0^{\infty} -\frac{dt(0,z)}{dz}\,dz\,. \tag{8.31}$$

The integral reduces to $t(0,0) - t^* = 1 - t^*$, yielding

$$I^{\downarrow}(0) = I^{\downarrow}(\infty)t^* + B(T_a)[1 - t^*]\,. \tag{8.32}$$

By the same token, (8.29)and (8.30) can be manipulated to yield

$$I^{\uparrow}(\infty) = I^{\uparrow}(0)t^* + B(T_a)[1 - t^*]\,. \tag{8.33}$$

Recall that the absorptivity of a nonscattering layer is just one minus the transmittance, and that Kirchhoff's Law states that absorptivity equals emissivity. The interpretation of the above two equations is thus remarkably simple: *The total radiant intensity is just the sum of*

(a)the transmitted intensity of any source on the far side plus (b) Planck's function times the emissivity of the entire atmosphere.

In reality, of course, the atmosphere is never isothermal. Nevertheless, it is sometimes convenient to use equations similar in form to (8.32) and (8.33) to describe the atmospheric contribution to the observed radiant intensity:

$$I^{\downarrow}(0) = I^{\downarrow}(\infty)t^* + \overline{B}^{\downarrow}[1 - t^*] \,, \tag{8.34}$$

$$I^{\uparrow}(\infty) = I^{\uparrow}(0)t^* + \overline{B}^{\uparrow}[1 - t^*] \,, \tag{8.35}$$

where

$$\overline{B}^{\downarrow} = \frac{1}{1 - t^*} \int_0^{\infty} B(z) W^{\downarrow}(z) \, dz \,, \tag{8.36}$$

$$\overline{B}^{\uparrow} = \frac{1}{1 - t^*} \int_0^{\infty} B(z) W^{\uparrow}(z) \, dz \,, \tag{8.37}$$

give the *weighted average* Planck function values for the entire atmosphere.

Problem 8.1: Show that when $1 - t^* \ll 1$, $W^{\downarrow}(z) \approx W^{\uparrow}(z) \approx \beta_a(z)/\mu$, so that $\overline{B}^{\downarrow} \approx \overline{B}^{\uparrow}$.

8.2.2 Monochromatic Flux †

Sometimes it is not the intensity but rather the flux that we care about. For example, if we ignore extraterrestrial sources (appropriate for the LW band), we can compute the downwelling monochromatic flux $F^{\downarrow}$ at the surface simply by integrating $I^{\downarrow} \cos\theta$ over one hemisphere of solid angle, according to (2.59):

$$F^{\downarrow} = -\int_0^{2\pi} \int_{\pi/2}^{\pi} I^{\downarrow}(\theta, \phi) \cos\theta \sin\theta \, d\theta d\phi.$$

There are two simplifications we can make before we even take the obvious step of substituting (8.27). First, in our plane parallel

atmosphere, nothing depends on ϕ; therefore we can immediately deal with the integration over azimuth, leaving

$$F^{\downarrow} = -2\pi \int_{\pi/2}^{\pi} I^{\downarrow}(\theta) \cos\theta \sin\theta \, d\theta \, . \tag{8.38}$$

Second, we can substitute $\mu = |\cos\theta|$ as our variable for describing zenith angle. For downwelling radiation, $\cos\theta < 0$, so in this instance $\mu = -\cos\theta$ and $d\mu = \sin\theta d\theta$; using (8.27), we are now able to write

$$F^{\downarrow}(0) = 2\pi \int_0^1 \left[\int_0^{\infty} B(z) W^{\downarrow}(z,\mu) \, dz \right] \mu d\mu \, . \tag{8.39}$$

Only $W^{\downarrow}$ depends on μ. Therefore, if we wish, we can reverse the order of integration and write

$$F^{\downarrow}(0) = \int_0^{\infty} \pi B(z) W_F^{\downarrow}(z) \, dz \, , \tag{8.40}$$

where

$$W_F^{\downarrow}(z) \equiv 2 \int_0^1 W^{\downarrow}(z,\mu) \mu \, d\mu = -2 \int_0^1 \frac{\partial t(0,z;\mu)}{\partial z} \mu \, d\mu \tag{8.41}$$

may be thought of as a *flux weighting function*. Hopefully, you will recognize the term $\pi B(z)$ appearing in (8.40) as the monochromatic flux you would expect from an opaque blackbody having the temperature found at altitude z. With a little more rearrangement, we can write

$$W_F^{\downarrow}(z) = -\frac{\partial}{\partial z} \left[2 \int_0^1 t(0,z;\mu) \mu \, d\mu \right] = -\frac{\partial t_F(0,z)}{\partial z} \, , \tag{8.42}$$

where the monochromatic *flux transmittance* t_F between levels z_1 and z_2 is defined as

$$t_F(z_1,z_2) \equiv 2 \int_0^1 t(z_1,z_2;\mu) \mu \, d\mu = 2 \int_0^1 e^{-\frac{\tau(z_1,z_2)}{\mu}} \mu \, d\mu \, . \tag{8.43}$$

Problem 8.2: Find expressions analogous to (8.40)–(8.42) for both the downwelling and upwelling flux at an arbitrary altitude z in the atmosphere.

Unfortunately, there is no simple closed-form solution to the integral in (8.43), though it is easily solved numerically. However, it turns out that the above expression for t_F behaves very much like the simple "beam" transmittance $t = \exp(\tau/\mu)$ — that is, it decreases quasi-exponentially from one to zero as τ goes from zero to infinity. Therefore, in order to deal with the integral, it is common to use the approximation

$$t_F = 2\int_0^1 e^{-\frac{\tau}{\mu}}\mu\, d\mu \quad \approx \quad e^{-\tau/\overline{\mu}}\,, \tag{8.44}$$

where $\overline{\mu}$ describes an *effective* zenith angle such that the corresponding beam transmittance is approximately equal to the flux transmittance between two levels.

Problem 8.3:
(a) Show that, for any specified value of τ in (8.44), there is always a value of $\overline{\mu}$ between zero and one that makes the relationship exact.
(b) Find an expression for $\overline{\mu}$ that is valid for the case that $\tau \ll 1$.

Although the "perfect" value of $\overline{\mu}$ is a function of τ, numerical experiments reveal that you can often get away with choosing a single constant value that yields a reasonable *overall* fit between the approximate expression

$$W_F^{\downarrow}(z) \approx -\frac{\partial t(0,z;\overline{\mu})}{\partial z}\,, \tag{8.45}$$

and the exact expression (8.42). The most commonly used value is $\overline{\mu} = 1/r$, where $r = 5/3$ is the so-called *diffusivity factor* that arises in certain theoretical analyses of the flux transmittance.

Problem 8.4: If you have access to software that can numerically evaluate integrals, then graph $t_F(\tau)$ for $0 < \tau < 2$. Compare your accurate results with those obtained using the above value for $\overline{\mu}$.

8.2.3 Surface Contributions to Upward Intensity

Equation (8.29) described the intensity of monochromatic radiation as seen looking downward from the top of the atmosphere. One of the terms appearing in this equation is the upward radiant intensity at the surface $I^{\uparrow}(0)$. This is the only term whose value cannot be directly computed from knowledge of $\beta_a(z)$ and $T(z)$ alone (for given wavelength λ and viewing direction μ). Therefore, in order to have a complete, self-contained expression for $I^{\uparrow}(\infty)$, it is necessary to find an explicit expression for $I^{\uparrow}(0)$.

The expression we supply for $I^{\uparrow}(0)$ depends on what we assume about the nature of the surface. But regardless of those assumptions, there are two contributions that must be considered: 1) emission by the surface itself, and 2) upward reflection of atmospheric radiation incident on the surface.

Specular Lower Boundary

Let us first consider the simplest possible case: that of a specular surface with emissivity ε. In this case, the reflectivity $r = 1 - \varepsilon$, and we have

$$I^{\uparrow}(0) = \varepsilon B(T_s) + (1 - \varepsilon) I^{\downarrow}(0) \,, \tag{8.46}$$

where T_s is the temperature of the surface (not necessarily the same as the surface *air* temperature!), and $I^{\downarrow}$ is evaluated for the same μ as $I^{\uparrow}$. Now recall that we have already derived an expression for $I^{\downarrow}(0)$, namely (8.27). Combining the latter with (8.29) and (8.46) yields:

$$\begin{aligned} I^{\uparrow}(\infty) = &\left[\varepsilon B(T_s) + (1 - \varepsilon) \int_0^{\infty} B(z) W^{\downarrow}(z)\, dz\right] t^* \\ &+ \int_0^{\infty} B(z) W^{\uparrow}(z)\, dz \,, \end{aligned} \tag{8.47}$$

where we have assumed that there is no extraterrestrial source of downward radiation in the direction of interest (i.e., we're not looking at the sun's reflection). Given the appropriate weighting functions $W^{\uparrow}$ and $W^{\downarrow}$, we have a self-contained expression for the radiant intensity that would be observed by a downward-viewing satellite sensor.

If we wish, we can use the notation developed in the previous subsection to hide the integrals:

$$I^{\uparrow}(\infty) = \left[\varepsilon B(T_s) + (1-\varepsilon)\overline{B}^{\downarrow}[1-t^*]\right] t^* + \overline{B}^{\uparrow}[1-t^*] \; . \tag{8.48}$$

There are three limiting cases of the above that help persuade us that our analysis makes sense. The first is that of a perfectly transparent atmosphere ($t^* = 1$), in which case our equation reduces to the expected dependence on surface emission alone:

$$I^{\uparrow}(\infty) = \varepsilon B(T_s) \; . \tag{8.49}$$

The second is that of a perfectly opaque atmosphere ($t^* = 0$), in which case surface emission and reflection are both irrelevant, and we have

$$I^{\uparrow}(\infty) = \overline{B}^{\uparrow} = \int_0^{\infty} B(z) W^{\uparrow}(z) \, dz \; . \tag{8.50}$$

The third occurs when the surface is nonreflecting; i.e., $\varepsilon = 1$, in which case we have

$$I^{\uparrow}(\infty) = B(T_s) t^* + \overline{B}^{\uparrow}[1-t^*] \; . \tag{8.51}$$

It would be tempting to interpret the last of these as showing a linear relationship between $I^{\uparrow}$ and atmospheric transmittance t^*, but remember that $\overline{B}^{\uparrow}$ also depends on the atmospheric opacity. In general, *as the atmosphere becomes more opaque, $\overline{B}^{\uparrow}$ represents emission from higher (and therefore usually colder) levels of the atmosphere.*

Lambertian Lower Boundary †

As discussed in Chapter 5, the "opposite" of specular reflection is a Lambertian reflection, for which radiation incident on the surface from any direction is reflected equally in all directions. When the

surface is Lambertian, the upward directed radiance at the surface $I^{\uparrow}(0)$ includes contributions due to the reflection of downwelling radiation from all possible directions. Combining (8.29) with (5.12), (5.14), and (8.41), we get

$$I^{\uparrow}(\infty,\mu) = \left[\varepsilon B(T_s) + 2(1-\varepsilon)\int_0^{\infty} \pi B(z) W_F^{\downarrow}(z)\, dz\right] t^* + \int_0^{\infty} B(z) W^{\uparrow}(z,\mu)\, dz\,, \tag{8.52}$$

where we have made the dependence of $W^{\uparrow}$ and $W^{\downarrow}$ on μ explicit.

Problem 8.5: Derive (8.52).

Problem 8.6: Equation (8.52) assumes there is no extraterrestrial source of radiation. Generalize it to include a columnated source (e.g., the sun) of monochromatic flux S (measured normal to the beam). The cosine of the zenith angle of the source is μ_0.

Problem 8.7: Equations (8.27)–(8.30) were derived for radiant intensities observed at the bottom and top of the atmosphere, respectively. Generalize these to describe the downward and upward intensities $I^{\downarrow}(z)$ and $I^{\uparrow}(z)$ at *any* arbitrary level z in the atmosphere. Include explicit expressions for the new weighting functions $W^{\downarrow}(z)$ and $W^{\uparrow}(z)$ in terms of $\beta_a(z)$, etc.

8.3 Applications to Meteorology, Climatology, and Remote Sensing

This chapter introduced the relationships that describe the transfer of monochromatic radiation in an atmosphere that doesn't *scatter*

appreciably but does *absorb* and *emit* radiation. When do these conditions apply?

As a general rule of thumb (see Chapter 12 for details), the longer the wavelength, the larger a particle has to be before it is capable of scattering appreciably. You can definitely neglect scattering by air molecules for wavelengths falling anywhere in the infrared or microwave bands. Cloud droplets and cloud ice particles continue to scatter appreciably throughout most of the near IR band, but in the thermal and far IR bands, water clouds (and to a lesser extent ice clouds) tend to look a lot like blackbodies. By the time you get to the microwave band, about the only particles for which scattering can't be neglected are precipitation particles — i.e., raindrops, snowflakes, hailstones, etc.

In short, you're *usually* safe using the relationships derived in this chapter throughout the thermal IR and microwave bands (excepting precipitation), while you're almost *never* safe using them in the solar (shortwave) part of the spectrum.

As you already know, the thermal IR band plays an extremely important role in the exchange of energy within the atmosphere, and between the atmosphere, the surface, and outer space. In principle, one might take the relationships we derived for monochromatic intensities and simply integrate them over both wavelength and solid angle in order to obtain broadband radiative fluxes at any level in the atmosphere. This is easier said than done, however, owing to the extreme complexity of the dependence of $\beta_a(z)$ on wavelength, as we shall see in Chapter 9. It is necessary to develop special methods for efficiently computing longwave (broadband) flux, and flux divergence, in the atmosphere. Some of these methods will be outlined in Chapter 10.

The relationships developed earlier in this chapter are therefore most directly useful in the context of infrared and microwave remote sensing. Most satellite sensors operating in these bands observe intensities rather than fluxes of radiation, and most do so for very narrow ranges of wavelength, so that in many cases the observed intensities can be thought of as quasi-monochromatic.

In the following, we will take a look at real-world atmospheric emission spectra and also outline the principles behind temperature and humidity profile retrieval. Since all of these topics are closely

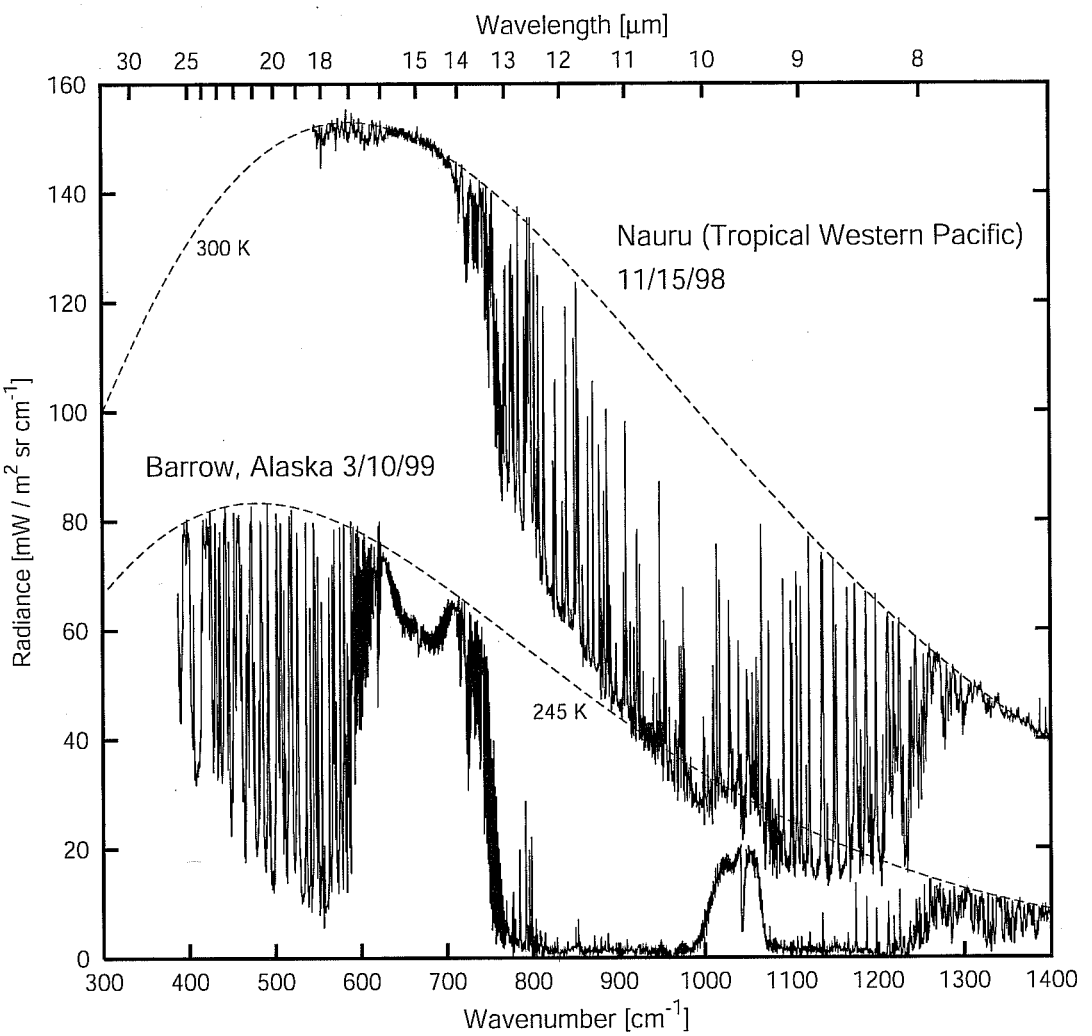

Fig. 8.1: Two examples of measured atmospheric emission spectra as seen from ground level looking up. Planck function curves corresponding to the approximate surface temperature in each case are superimposed (dashed lines). *(Data courtesy of Robert Knuteson, Space Science and Engineering Center, University of Wisconsin-Madison.)*

tied to the absorption spectra of various atmospheric constituents, you might find it helpful to go back and review the major absorption bands depicted in Fig. 7.6.

8.3.1 The Spectrum of Atmospheric Emission

A *spectrometer* is a device that measures radiant intensity as a function of wavelength. Infrared spectrometers have been deployed on satellites, which view the atmosphere looking down from above, and at fixed and mobile research stations on the ground, where they

can measure the atmospheric emission spectrum reaching the surface. In addition, spectrometers are occasionally flown on research aircraft. The latter may view downward, upward, or both.

For an upward-viewing instrument at ground level, the relevant form of the radiative transfer equation is given most generally by (8.27), but here we will assume that there are no extraterrestrial sources of radiation:

$$I^{\downarrow}(0) = \int_0^{\infty} B(z) W^{\downarrow}(z) dz \, . \tag{8.53}$$

For a satellite sensor viewing downward, we have

$$I^{\uparrow}(\infty) = B(T_S) t^* + \int_0^{\infty} B(z) W^{\uparrow}(z) dz \, , \tag{8.54}$$

where we are assuming that the surface is nonreflective and has temperature T_S, so that $I^{\uparrow}(0) = B(T_S)$.

For the sake of the discussion to follow, we needn't worry about the detailed shape of the weighting functions $W^{\uparrow}(z)$ and $W^{\downarrow}(z)$. The important thing to remember is that when the atmosphere is very opaque, the measured radiation will be due principally to emission from the nearest levels of the atmosphere; when it is less opaque, the relevant weighting function will include emission from more remote levels. Finally, when the atmosphere is *very* transparent, the instrument will "see through" the atmosphere, measuring primarily the radiance contribution (if any) from the far side — e.g., the surface for a downward-looking instrument or "cold space" for an upward-looking one.

Of course, no matter what the source of the measured radiance, we can always interpret that radiance as a brightness temperature T_B, according to (6.13). If the atmosphere happens to be opaque at a particular wavelength, then the brightness temperature in turn gives you a reasonable estimate of the physical temperature at the level where the weighting function peaks.

Figure 8.1 shows a pair of relatively high-resolution IR spectra measured at ground level under two different sets of conditions. One was taken at a location in the tropical western Pacific, where atmospheric temperatures are warm and humidity is high. The other was taken at an arctic location in late winter, where temperatures

are very cold and the atmosphere contains only small amounts of water vapor. Both were taken under cloud-free skies.

As complicated as these spectra appear to the untrained eye, the interpretation is really rather simple. Let's take it one step at a time.

- The two dashed curves depict the Planck function at temperatures representative of the *warmest* atmospheric emission seen by the instrument at each location. At the tropical site, this is 300 K; at the arctic site, it's 245 K. Note that these curves serve as an approximate *upper bound* to the radiance measured in any wavelength band.

- In the tropical case, there are two spectral regions for which the measured radiance is very close to the reference curve at 300 K. One is associated with $\lambda > 14$ μm ($\tilde{\nu} < 730$ cm^{-1}); the other with $\lambda < 8$ μm ($\tilde{\nu} > 1270$ cm^{-1}). In both of these bands, we can infer that the atmosphere must be quite opaque, because virtually all of the observed radiation is evidently being emitted at the warmest, and therefore lowest, levels of the atmosphere. Referring to Fig. 7.6 in section 7.4.1, we find that these features are consistent with (a) strong absorption by CO_2 in the vicinity of 15 μm, (b) strong absorption by water vapor at wavelengths longer than 15 μm, and (c) strong absorption by water vapor between 5 and 8 μm.

- The two water vapor absorption bands mentioned above are also evident in the arctic emission spectrum (for which the measurements extend to a somewhat longer maximum wavelength of 25 μm). However, because the atmosphere is so dry in this case, these bands are not as uniformly opaque and therefore the measured radiance is quite variable. In fact, between 17 and 25 μm, the general impression is of a large number of strong water vapor lines separated by what might be termed "microwindows." The most transparent of the latter is found near 18 μm (560 cm^{-1}).

- Between 8 and 13 μm in the tropical spectrum, observed brightness temperatures are considerably colder than the surface, and in some cases as cold as 240 K. This broad region may be regarded as a "dirty window" — the atmosphere overall is

fairly transparent, but there are a large number of individual absorption lines due to water vapor.

- In the arctic spectrum, the above window "opens up" substantially, because there is far less water vapor in the atmospheric column to absorb and emit radiation. Therefore, observed radiances between 8 and 13 μm are generally quite low indeed — the instrument effectively has an unobstructed view of cold space.

- A clear exception to the above statement is found between 9 and 10 μm. Referring again to Fig. 7.6, we infer that the culprit this time is the ozone absorption band centered at 9.6 μm. This band, while not totally opaque, emits sufficiently strongly to raise the brightness temperature to around 230 K, much warmer than the surrounding window region. The "cold" spike at the center of the ozone band corresponds to an isolated region of relative transparency.

- Carefully examining the tropical emission spectrum, we discover that the 9.6 μm ozone band is apparent there as well. But because the surrounding window is much less transparent in this case, the ozone band does not stand out nearly as strongly.

- Now let's take a closer look at the CO_2 band in the arctic spectrum. At 15 μm, the measured brightness temperature of approximately 235 K is significantly *colder* than it is on the edges of the band near 14 and 16 μm, where the brightness temperature is close to the maximum value of 245 K. Yet we know that at the center of the band, where absorption is the strongest, the emitted radiation should be originating at the levels closest to the intrument, namely in the lowest few meters of the atmosphere. How do we explain this apparent paradox? In fact, there is no paradox; we are simply witnessing the effects of a strong *inversion* in the surface temperature profile — i.e., a sharp *increase* in temperature with height in the lowest few hundred meters of the atmosphere.[3] At the center of the CO_2

[3]Deep surface inversions, relatively uncommon elsewhere, are the rule in wintertime polar regions.

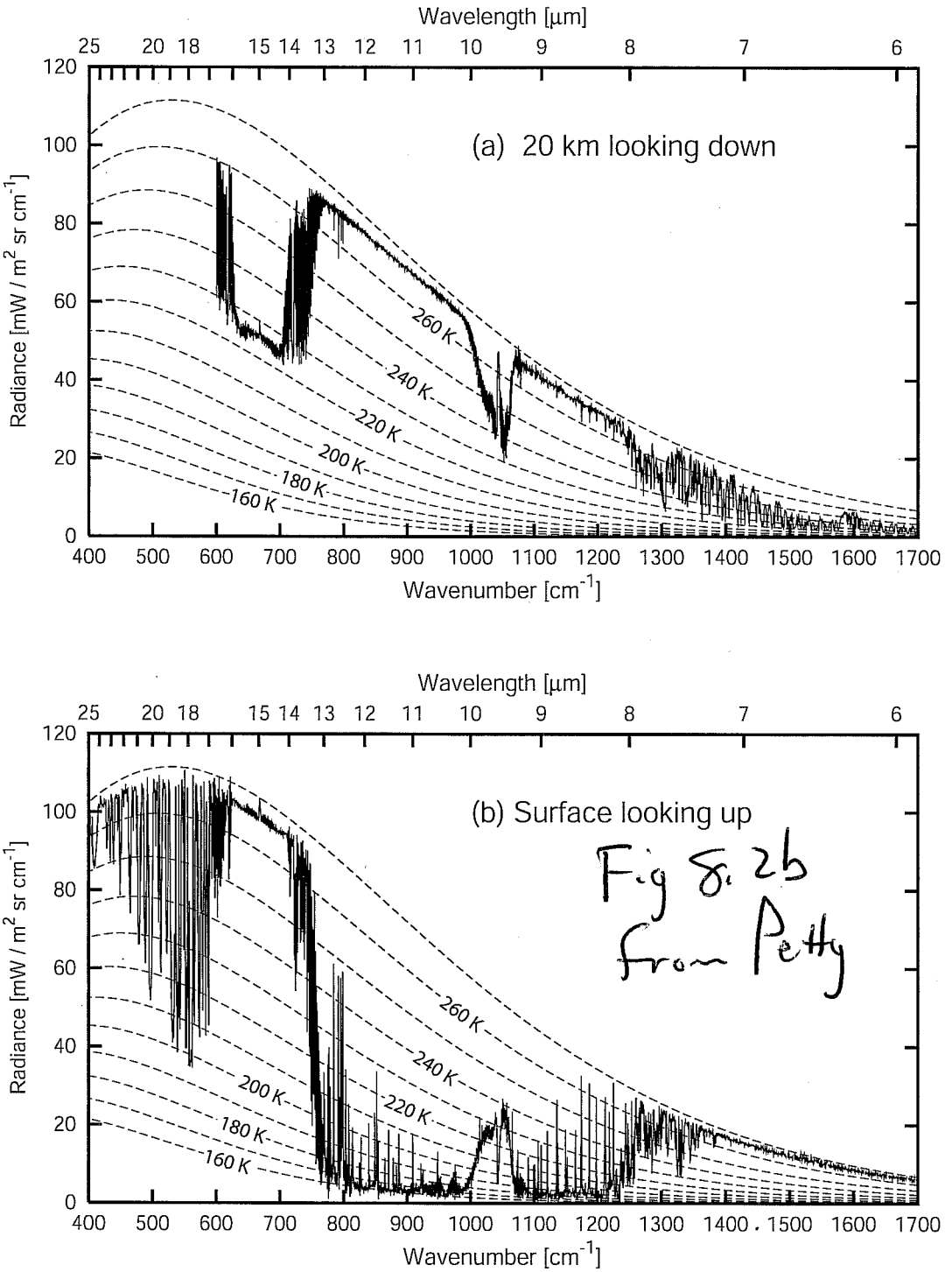

Fig. 8.2: Coincident measurements of the infrared emission spectrum of the cloud-free atmosphere at (a) 20 km looking downward over the polar ice sheet and (b) at the surface looking upward. *(Data courtesy of David Tobin, Space Science and Engineering Center, University of Wisconsin-Madison.)*

band, the spectrometer records emission from the coldest air right at the surface. At the edges of the band, where the air is less opaque, it sees emission from the warmer layer of air at the top of the inversion. This example hints at the possibility of using remote measurements of atmospheric emission to infer atmospheric temperature structure. We will return to that topic shortly.

Let's now take a look at how the atmospheric emission spectrum changes depending on whether you are looking down from above or looking up from the surface. Fig. 8.2 gives us a rare opportunity to compare the two perspectives for the same atmospheric conditions: an aircraft flying at 20 km altitude measured the upwelling emission spectrum at exactly the same time and location as a surface instrument looking up measured the downwelling spectrum. The measurements in this case were taken over the arctic ice pack and are therefore comparable in some respects to the arctic spectrum already discussed. The following exercise asks you to provide the physical interpretation:

Problem 8.8: Based on the measured spectra depicted in Fig. 8.2, answer the following questions: (a) What is the approximate temperature of the surface of the ice sheet, and how do you know? (b) What is the approximate temperature of the near-surface *air*, and how do you know? (c) What is the approximate temperature of the air at the aircraft's flight altitude of 20 km, and how do you know? (d) Identify the feature seen between 9 and 10 μm in both spectra. (e) In Fig. 8.1, we saw evidence of a strong inversion in the near-surface atmospheric temperature profile. Can similar evidence be seen in Fig. 8.2? Explain.

We'll conclude our discussion of atmospheric emission spectra by looking at examples of satellite observations made under diverse conditions around the globe (Fig. 8.3). Once again, I'll leave most of the physical interpretation as an exercise. Only one new point requires a brief explanation, because it didn't arise in our previous discussion of surface- and aircraft-measured spectra. That concerns the prominent narrow spike observed at the center of the 15 μm CO_2 band in all four panels. This spike occurs where absorption is by far

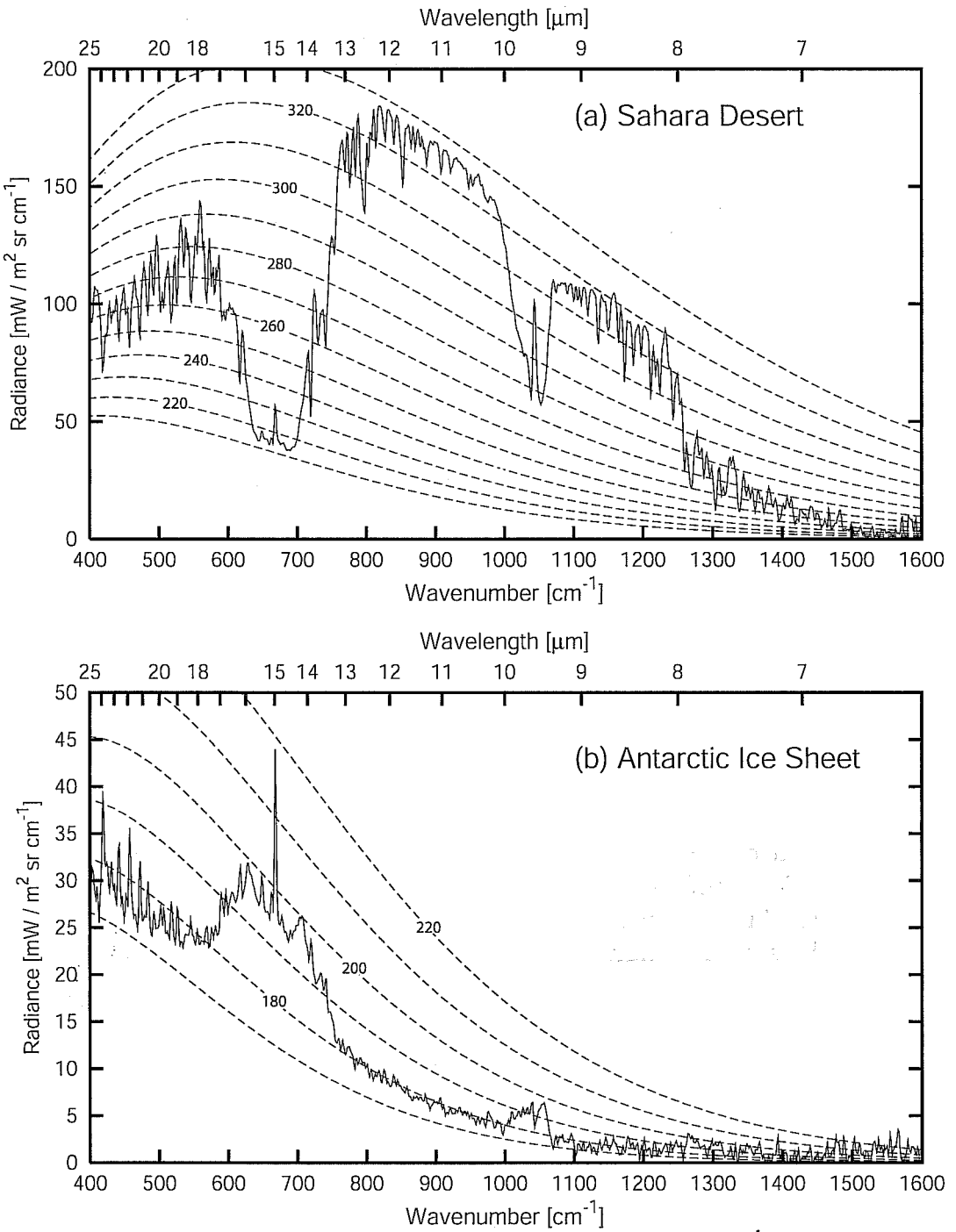

Fig. 8.3: Examples of moderate resolution IR spectra observed by a satellite spectrometer. Except for the curve labeled "thunderstorm anvil" in panel (c), all spectra were obtained under cloud-free conditions. *(Nimbus-4 IRIS data courtesy of the Goddard EOS Distributed Active Archive Center (DAAC) and instrument team leader Dr. Rudolf A. Hanel.)*

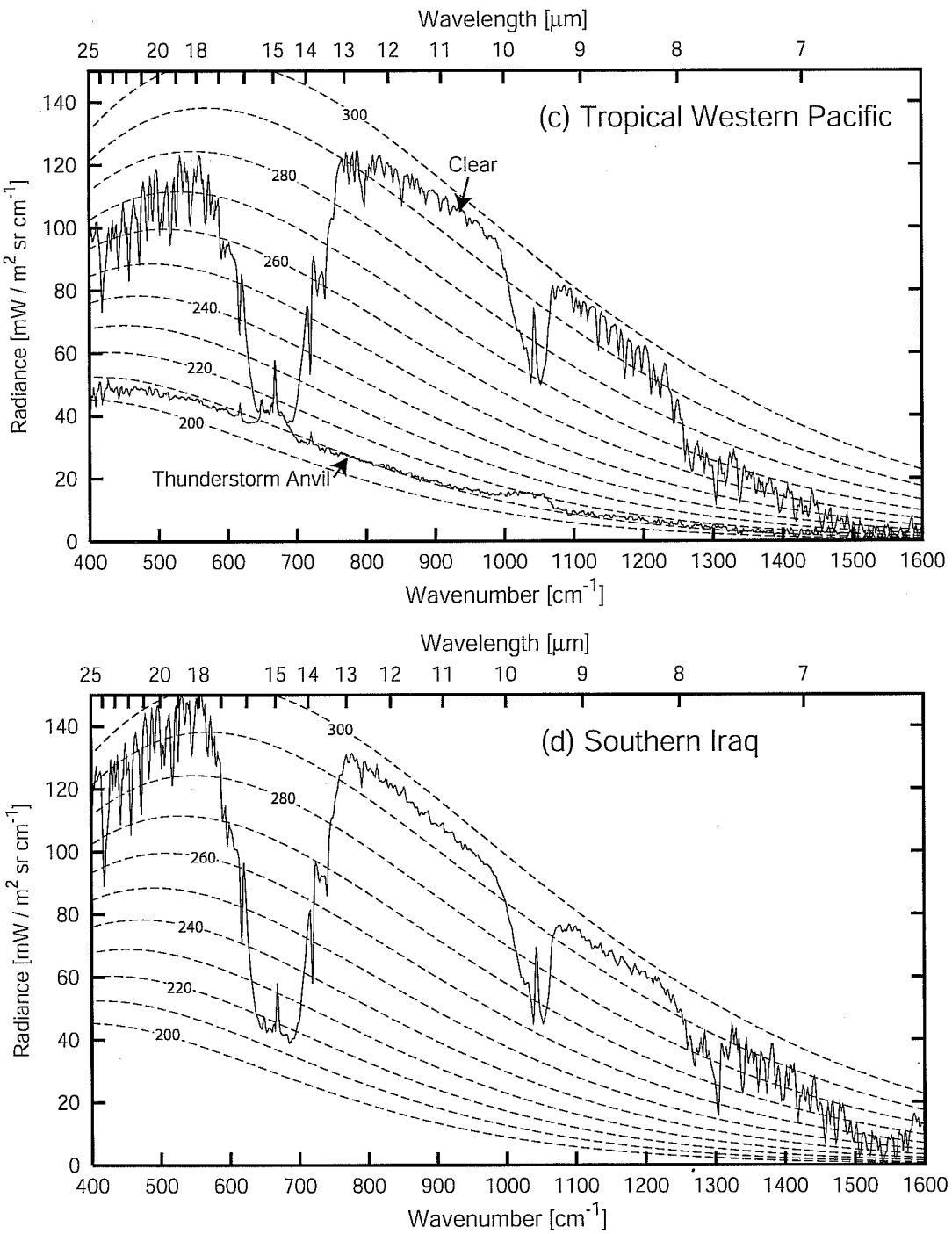
Wavelength [μm]
25 20 18 15 14 13 12 11 10 9 8 7
(c) Tropical Western Pacific
Clear
Thunderstorm Anvil
300
280
260
240
220
200
Radiance [mW / m² sr cm⁻¹]
Wavenumber [cm⁻¹]
(d) Southern Iraq

Fig. 8.3: (cont.)

the most intense of any point in the thermal IR band. From the vantage point of a satellite sensor viewing downward, emission at this wavelength therefore originates almost entirely in the stratosphere, whereas most of the remaining emission spectrum is associated primarily with the surface and troposphere.[4]

To summarize, as you move from the edge of the CO_2 band toward the center, the general tendency for satellite-observed spectra is *usually*: (i) decreasing brightness temperature as the emission weighting function $W^{\uparrow}$ peaks at higher (and colder) levels in the troposphere, followed by (ii) a sharp reversal of this trend at the strongly absorbing center of the band, where the weighting function peaks at an altitude solidly within the relatively warm stratosphere.

Problem 8.9: Contrast the above explanation for the narrow warm spike at the center of the 15 μm CO_2 band with the explanation for the similar-appearing warm spike at the center of the 9.6 μm ozone band, as seen in several panels of Fig. 8.3.

Problem 8.10: Referring to Fig. 8.3, answer each of following questions.

(a) For each of the four scenes, provide an estimate of the surface temperature.

(b) For which scene does the surface appear to be significantly colder than any other level in the atmosphere?

(c) Compare the apparent humidity of the atmosphere over Southern Iraq with that over the Sahara Desert, and explain your reasoning.

[4]The *troposphere* is the layer of the atmosphere closest to the surface and is usually characterized by decreasing temperature with height. The troposphere is typically anywhere from a few km to 15 km deep, depending on latitude and season. The *stratosphere* is the deep layer above the troposphere in which temperature generally increases with height. The boundary between the troposphere and the stratosphere, called the *tropopause*, is often (though not always) the coldest point in the atmospheric temperature profile below 40 km. The layer of highest ozone concentration is found in the stratosphere between 15 and 30 km. If these facts are new to you, then I recommend that you spend an evening with Chapter 1 of WH77 and/or Section 3.1 of L02.

(d) Estimate the temperature of the thunderstorm cloud top in the Tropical Western Pacific. Why is this emission spectrum so much smoother than that for the neighboring clear atmosphere? Explain the small variations in brightness temperature that *do* show up.

(e) Explain why the ozone band at 9.6 μm shows up as a relatively warm feature in the Antarctic spectrum, but a relatively cold feature for all other scenes.

8.3.2 Satellite Retrieval of Temperature Profiles

As we have seen in Sections 7.4.1 and 8.3.1, certain atmospheric constituents — most notably CO_2, water vapor, ozone, and oxygen — are associated with strong absorption lines and bands that render the atmosphere opaque over certain ranges of wavelengths. Some of these constituents, such as CO_2 and O_2 are "well mixed" throughout the troposphere and stratosphere. That is, they are present at a constant, accurately known mass ratio w to all other constituents of the atmosphere. If you knew the density profile $\rho(z)$ of the atmosphere, then the density of the absorbing constituent would just be $\rho'(z) = w\rho(z)$. If you also knew the mass absorption coefficient $k_a(z)$ of the constituent, then you could calculate the optical depth $\tau(z)$ and thus the emission weighting function $W^{\uparrow}(z)$ that appears in the integral in (8.29).

The relative strength of absorption at the wavelength in question determines whether $W^{\uparrow}(z)$ will peak at a high or low altitude in the atmosphere. If you build a satellite sensor that is able to measure the radiant intensities I_λ for a series of closely spaced wavelengths λ_i located on the edge of a strong absorption line or band for the constituent (e.g., near 15 μm for CO_2), each channel will measure thermal emission from a different layer of the atmosphere. The closer the wavelength is to the line center, the higher in the atmosphere the weighting function will peak. The intensity of the emission is of course determined by the atmospheric temperature within that layer.

In principle, you can find a temperature profile $T(z)$ that is simultaneously consistent with each of the observed radiances I_λ for the scene in question. Typically, you would start with a "first guess"

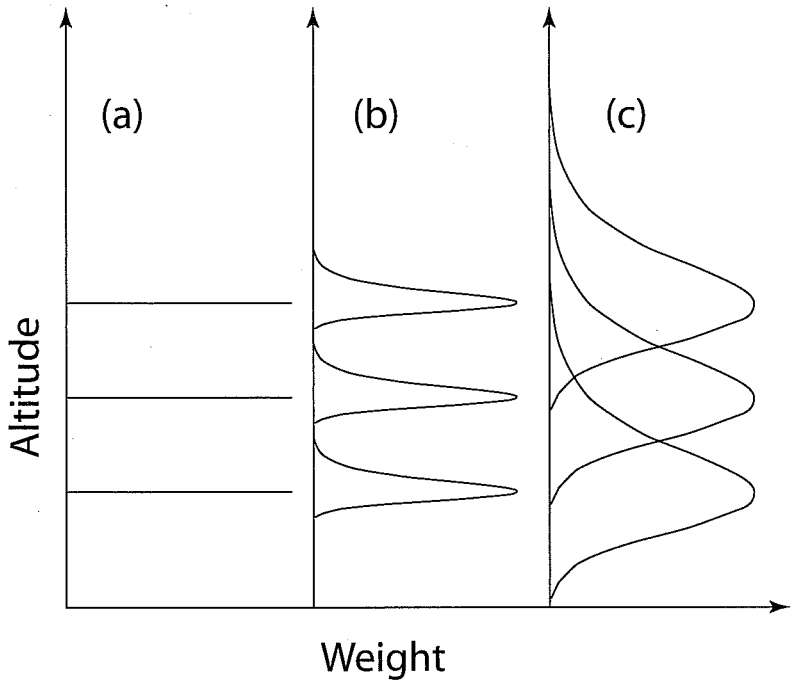

Fig. 8.4: Idealized satellite sensor weighting functions for atmospheric temperature profile retrievals. (a) Channel weighting functions resemble δ-functions; i.e., all emission observed by each channel originates at a single altitude. (b) Observed emission represents layer averages, but channel weighting functions do not overlap. (c) Realistic case, in which weighting functions not only represent layer averages but also overlap.

profile and compute the associated intensities for each channel using (8.29). You would then compare the computed intensities with the observed intensities and adjust the profile in such a way as to reduce the discrepancies. This process could be repeated until the differences for all channels fell to within some tolerance, based on the assumed precision of the instrument measurements themselves and of the model calculations of I_λ.

The above procedure (with certain important caveats; see below) is in fact not too far from that actually used in routine satellite-based temperature profile retrievals. It is not my purpose here to embark on a rigorous discussion of remote sensing theory, which is best left for a separate course and/or textbook. It is enough for now that you recognize the close connection between the radiative transfer principles discussed earlier in this chapter and an application of immense practical importance to modern meteorology.

Figure 8.4 depicts the physical basis for profile retrieval at three levels of idealization, starting with the simplest — and least realis-

tic — on the left: If weighting functions happened to be perfectly sharp — that is, if all emission observed at each wavelength λ_i originated at a single altitude (Fig. 8.4a), then "inverting" the observations would be simple: in this case, the observed brightness temperatures $T_{B,i}$ would exactly correspond to the physical temperatures at the corresponding altitudes h_i. Your job is then essentially finished without even lifting a calculator. Of course, you wouldn't know how the temperature was varying *between* those levels, but you could either interpolate between the known levels and hope for the best or, if your budget was big enough, you could add an arbitrary number of new channels to your sensor to fill in the vertical gaps.

Slightly more realistically, panel (b) depicts the weighting functions as having finite width, so that the observed brightness temperatures correspond to an *average* of $B_\lambda[T(z)]$ over a substantial depth of the atmosphere rather than a unique temperature T_i at altitude h_i. There is now ambiguity in the retrieval, because there is no single atmospheric level that is responsible for all of the emission measured by any given channel. At best, you can estimate the *average layer temperature* associated with each channel. Nevertheless, the profile retrieval problem itself remains straightforward, because each channel contains completely independent information: there is no overlap between the weighting functions.

Unfortunately, real weighting functions are constrained to obey the laws of physics, as embodied in (8.30). This means that unless you have an unusually sharp change with altitude in the atmospheric absorption coefficient β_a, your weighting functions will be quite broad. In the worst case, the mass extinction coefficient k_a of your chosen constituent will be nearly constant with height, so that the weighting functions will be essentially those predicted for an exponential absorption profile as discussed in Section 7.4.3. The situation is somewhat better for sensor channels positioned on the edge of an absorption line (or between two lines), because *pressure broadening* (see Chapter 9) then increases k_a toward the surface, which sharpens the weighting function. Nevertheless, the improvement is not spectacular.

Therefore, given any reasonable number of channels, there is always considerable overlap between adjacent weighting functions,

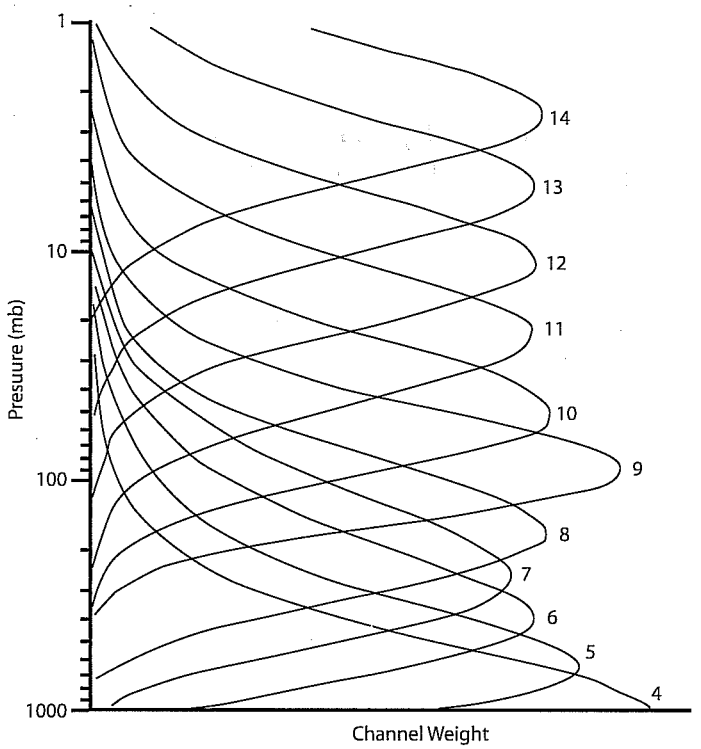

Fig. 8.5: Weighting functions for channels 4–14 of the Advanced Microwave Sounding Unit (AMSU).

as depicted schematically in Fig. 8.4c. In fact, Fig. 8.5 shows actual weighting functions for the Advanced Microwave Sounding Unit (AMSU), which has 11 channels on the edge of the strong O_2 absorption band near 60 GHz (c.f. Fig. 7.7). Although each satellite sounding device has its own set of channels and therefore its own unique set of weighting functions, those for the AMSU are fairly typical for most current-generation temperature sounders in the infrared and microwave bands.

To summarize: It is clear on the one hand that there is information about vertical temperature structure in the radiant intensities observed by a sounding instrument like the AMSU. On the other hand, one shouldn't underestimate the technical challenge of retrieving temperature profiles of *consistently useful quality* from satellite observations. In outline form, here are the main issues:

- In general, it takes far more variables to accurately describe an arbitrary temperature profile $T(z)$ than there are channels on a typical satellite sounding unit. This means that you have fewer measurements than unknowns, and the retrieval prob-

lem is *underdetermined* (or *ill-posed*). The problem is therefore not just that of finding any temperature profile that is consistent with the measurements; the real problem is of choosing the *most plausible* one out of an infinity of physically admissible candidates.

- Because of the high degree of vertical overlap between adjacent weighting functions, the temperature information contained in each channel is not completely independent from that provided by the other channels. That is to say, if you have N channels, you don't really have N independent pieces of information about your profile; you have something *less* than N, which makes the problem highlighted in the previous paragraph even worse that it appears at first glance.

- Because any measurement is inherently subject to some degree of random error, or *noise*, it is important to undertake the retrieval in such a way that these errors don't have an excessive impact on the final retrieved profile.

- Because of the large vertical width of the individual weighting functions, a satellite's view of the atmosphere's temperature structure is necessarily very "blurred" — that is, it is impossible to resolve fine-scale vertical structure in the temperature profile. As a consequence, a great many of the candidate profile solutions that would be *physically consistent* with the observed radiances $I_{\lambda,i}$ exhibit wild oscillations that are completely inconsistent with any reasonable temperature structure of the atmosphere. Effectively weeding out these bad solutions while retaining the (potentially) good ones requires one to impose requirements on the "smoothness" of the retrieved profile or limits on the allowable magnitude of the departure from the "first guess" profile.

Of course, well-established methods exist for dealing with the above challenges, and satellite temperature profile retrievals are successfully obtained at thousands of locations around the globe every day. These retrievals provide indispensable information about the current state of the atmosphere to numerical weather prediction models. Without the availability of satellite-derived temperature

structure data, accurate medium- and long-range forecasts (three days and beyond) would be impossible almost everywhere, and even shorter-range forecasts would be of questionable value over oceans and other data sparse regions.

8.3.3 Water Vapor Imagery

In the previous subsection, we looked at the case that satellite-observed emission was associated with a constituent that was "well-mixed" in the atmosphere. Under that assumption, the vertical distribution of the absorber is essentially known, and variations in brightness temperature can be attributed to variations in temperature in the atmospheric layer associated with each channel.

One can also imagine the opposite situation, in which the temperature profile is reasonably well known (perhaps from satellite measurements, as described above), but the concentration of the absorbing/emitting constituent is unknown and highly variable in both time and space. Such is the case for infrared images acquired at wavelengths between about 5 and 8 μm, where atmospheric emission and absorption is very strong in connection with the water vapor band centered at 6.3 μm.

The wavelength in this band most commonly utilized for satellite imaging is 6.7 μm, where water vapor absorption is strong enough to block surface emission from reaching the satellite under most conditions, but weak enough that the imager can usually "probe" well into the troposphere without being blocked by the small amounts of water vapor found in the stratosphere and upper troposphere.

Unlike the case for CO_2 and O_2, water vapor is far from well mixed and varies wildly in concentration, both horizontally and vertically. Therefore, the emission weighting function $W^{\uparrow}$ at 6.7 μm is highly variable, peaking at low altitudes (or even the surface) in a very dry atmosphere and in the upper troposphere in a humid tropical atmosphere or when high altitude clouds are present.

As usual, the observed brightness temperature T_B is a function of the temperature of the atmosphere in the vicinity of the weighting function peak, but variations in brightness temperature are a much stronger function of height of the weighting function peak than of

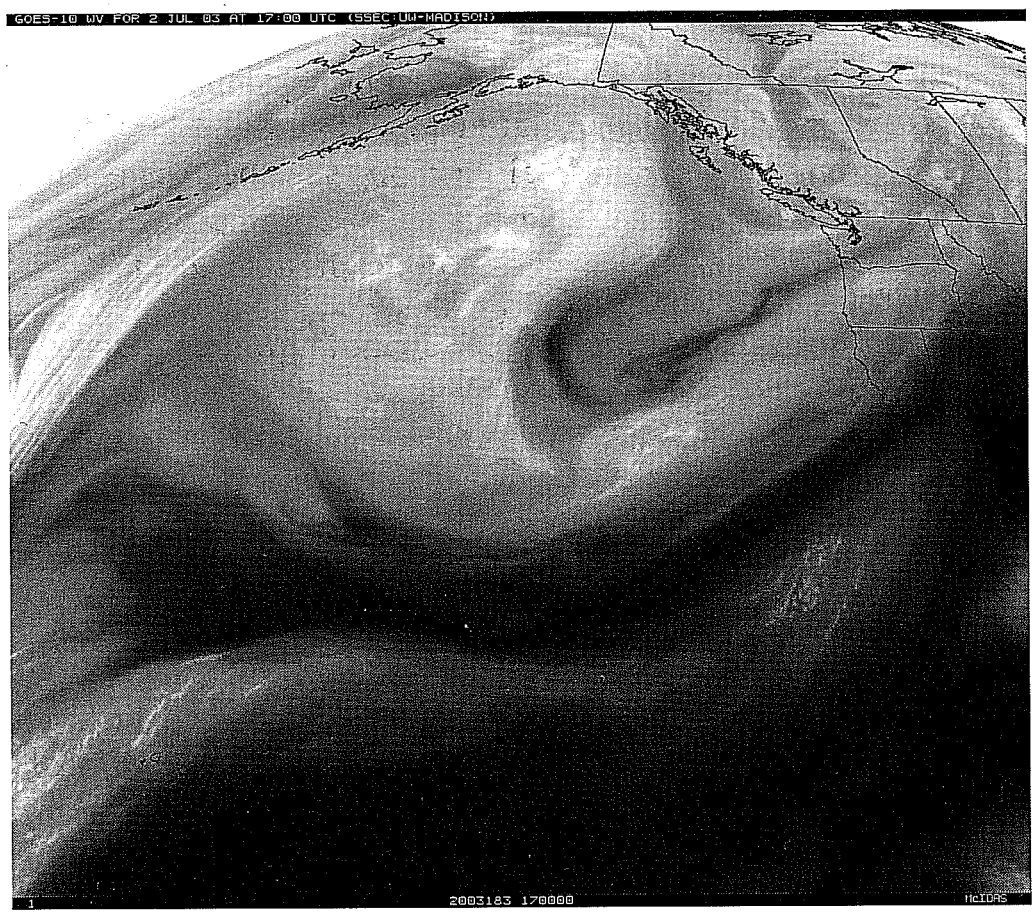

Fig. 8.6: An image of the Eastern Pacific and west coast of North America taken by the GOES-West geostationary weather satellite at a wavelength of 6.7 μm. This wavelength falls within the strong water vapor absorption band centered on 6.3 μm.

the temperature at any specific altitude.

Consequently *dry*, cloud-free air masses typically produce relatively *warm* brightness temperatures, because the observed emission originates at the warm lower levels of the atmosphere. *Humid* air masses, on the other hand, produce *cold* brightness temperatures, because emission then originates principally in the cold upper troposphere. In fact, globally speaking, there is often a roughly inverse correlation between brightness temperature at 6.7 μm and air mass temperature, because warm tropical air masses are capable of supporting higher water vapor content, and may also be associated with colder tropopause temperatures, on average, than cold extratropical air masses.

An example of a 6.7 μm image is shown in Fig. 8.6. In this in-

stance, the most dramatic features are the very dark (warm) bands snaking across the subtropical Pacific. These bands are presumably associated with regions of strong subsidence (sinking motion) in connection with the subtropical high pressure belt. The effect of subsidence is to bring extremely dry air from the upper troposphere down to relatively low levels, allowing the imager to "see" warm emission from the lowest kilometer or two. Elsewhere, deep humidity and some high-level clouds connected with a weakening extratropical cyclone produce bands of relatively cold brightness temperatures. Overall, one has an impression of a three-dimensional "surface" representing the upper boundary of the most humid layer of the atmosphere. This humidity structure is of course invisible in the conventional visible and IR images shown previously for the same time (Figs. 5.6 and 6.9).

Because the observed brightness temperature depends both on the amount and detailed vertical distribution of water vapor present and on the temperature structure of the atmosphere, it is generally not possible to retrieve quantitative humidity information using this channel alone. However, if you have several channels with varying sensitivity to water vapor absorption, they can be used in combination with temperature sounding channels to obtain vertical profiles of humidity. Of course, the same practical difficulties that were outlined for the temperature profile retrieval problem are encountered here as well. If anything, they are worse, because there are few useful criteria for distinguishing a "realistic" from an "unrealistic" humidity profile, except for the need to avoid supersaturation. Also, because the temperature profile cannot be retrieved with perfect precision, errors in this profile "feed through" to the humidity profile retrieval and constitute an additional source of error.